A high throughput, linear molecular beam epitaxy system for reduced cost manufacturing of GaAs photovoltaic cells: Will GaAs ever be inexpensive enough?

Journal:	*Sustainable Energy & Fuels*
Manuscript ID	SE-ART-12-2019-001255.R1
Article Type:	Paper
Date Submitted by the Author:	14-Feb-2020
Complete List of Authors:	Lee, Byungjun; University of Michigan, EECS Fan, Dejiu; University of Michigan, EECS Forrest, Stephen; University of Michigan, EECS

SCHOLARONE™
Manuscripts

A high throughput, linear molecular beam epitaxy system for reduced cost manufacturing of GaAs photovoltaic cells: Will GaAs ever be inexpensive enough?

Byungjun Lee[1], Dejiu Fan[1], and Stephen R. Forrest[1,2]

[1]Department of Electrical Engineering and Computer Science, University of Michigan, Ann Arbor, MI 48109

[2]Departments of Physics and Materials Science and Engineering, University of Michigan, Ann Arbor, MI 48109

Abstract

Solar cells based on GaAs and related compounds provide the highest reported efficiency single junction and multijunction solar cells. However, the cost of the cells is prohibitive when compared with Si and other thin film solar technologies. One significant differentiator is the high cost required to grow the epitaxial layers. Here, we propose a molecular beam epitaxy (MBE) system design that has the potential to increase the epitaxial layer growth throughput, thereby significantly reducing production costs. A rack-and-pinion based linear transfer system sequentially transfers multiple substrate platens between interconnected growth positions within the chamber, thereby synchronously growing layers on many wafers in the desired order and at the required thicknesses. The proposed linear MBE platform is the basis for a realistic analysis of GaAs single junction photovoltaic cell production cost. Our model projects a nearly 55% cost reduction in epitaxial growth via linear MBE when compared to conventional MBE, and a 85% reduction when further process optimization is assumed and combined with non-destructive epitaxial lift off. Even when considering all of these factors in an optimistic light, the cost of unconcentrated GaAs solar cells using *any* existing growth process is unlikely to drop below $3/Wp in the foreseeable future.

I. Introduction

Despite the high power conversion efficiency (*PCE*) of GaAs photovoltaic cells,[1] their widespread adoption for solar-to-electricity energy conversion has been limited due to the exceptionally high cost of materials and epitaxial growth of the active solar cell layers. Several different approaches have been engineered to reduce the cost of GaAs photovoltaic cells, such as substrate recycling through epitaxial lift-off (ELO) followed by wet and dry etching of a substrate recovery layer[2–5] or chemical mechanical polishing (CMP).[6–8] Controlled spalling by removal of a surface layer from the substrate using an intervening stress layer[9,10] could potentially be an alternative substrate useful in recycling, although it can result in a rough wafer surface.[9,10] Use of low-cost, non-III-V substrates such as Si or Ge[11,12] is also considered a potential pathway to cost reduction, although the performance of GaAs cells remains poor due to dislocations formed from lattice mismatch during growth.[13,14] Besides substrate recycling, the expensive photovoltaic active cell area can be reduced by the use of low-cost concentrators.[4,15] However, none of these approaches alone can effectively reduce the cost to levels that approach Si photovoltaics due to the limited number of substrate reuses through ELO[2,3] or the complexity and cost of concentrator tracking systems.[16] Moreover, the cost of ownership of GaAs epitaxial growth equipment such as metal-organic chemical vapor deposition (MOCVD) or molecular beam epitaxy (MBE), contributes substantially to the solar cell cost.[7,17] This is due, in part, to the low throughput of the epitaxial growth technology for MBE, or the use of costly, highly refined chemical precursors for MOCVD. Analysis of the manufacturing costs of a single junction GaAs cell based on MOCVD [7] predicts the cost of GaAs cells can be as low as $3.50 - $4.50/Wp, with an optimized cell structure, >50 epitaxial lift off cycles from a single wafer, and unspecified improvements of growth technology and reductions in materials cost. This is compared to the current, approximately

$80/Wp where only a handful of ELO steps are employed using conventional growth and fabrication methods. Another analysis of the costs of dual junction GaInP/GaAs solar cells grown by so-called dynamic hydride vapor phase epitaxy (D-HVPE)[18] also claims an optimistic reduction of GaAs cell cost to $2.00 - $3.00/Wp via increased wafer throughput using a potentially high growth rate of 200-300 μm/hr for GaAs[19] and 50 μm/hr for GaInP.[20] However, some of the assumptions for both cases are yet to be specified, such as improved material utilization, use of inexpensive yet-to-be-identified growth future precursors for MOCVD. Also, one critical cost reduction comes from unspecified future wafer cost reductions that rely heavily on improved substrate reuse of > 50 times, although current demonstrations remain near < 5.[2,3] Furthermore, the rapid HVPE growth of some alloys needed in high efficiency and low cost III-V solar cells necessary to enable ELO (e.g. AlAs) remains problematic.

Here, we propose a high throughput linear MBE (LMBE) system that can reduce costs even further than is realized using multiple wafer recycles via the recently introduced process of non-destructive ELO (ND-ELO).[2–4,15] The objective underlying this proposal is to determine whether GaAs solar cells costs are primarily driven by capital expenses related to a particular growth technology, or by other potentially less cost-elastic sources. While conventional MBE is a proven technology for the growth of high quality III-V solar cells using pure elemental (and hence relatively low cost) source materials, its exceptionally low growth rates (1 -3 μm/hr) severely limit wafer throughput. This has led to prohibitively high capital expense that has prevented its use in relatively low cost solar cell manufacturing. The LMBE design considered here alleviates some of these concerns by replacing a single, multi-purpose growth chamber with a continuous line of interconnected chambers, each whose purpose is to grow a separate layer needed in the solar cell structure. The in-line system is connected at opposite ends by rapid wafer loading and unloading

chambers. Realistic production costs of archetype single junction GaAs solar cells based on modified, previous estimates of the cost of MOCVD growth[7] using this tool are estimated.

Our analysis shows the solar-to-electricity energy conversion cost using GaAs thin film photovoltaic cells is reduced from \$24.82/Wp for conventional MBE, to \$13.63/Wp, using LMBE. With further optimized processes such as ND-ELO, the cost can be reduced to \$3.67/Wp. A comparative analysis of growth by LMBE, MOCVD and D-HVPE indicates that all processes are projected to yield approximately the same cost-per-Watt for GaAs solar cells, indicating that the capital expense of these three growth methods is less of a factor in determining cell cost than the cost of materials and fabrication processes. However, savings from improved throughput is independent of reductions in substrate cost, which is primarily determined by the efficacy of the substrate reuse technology. We conclude that even under the *most optimistic* assumptions made for growth, processing conditions, and cell configurations, the cost of GaAs-based solar cells is over ten times that of current Si solar cells, and will remain as such for the foreseeable future.[21]

II. Linear MBE System Design: Reducing the cost of epitaxial growth

A schematic top view of a conventional, production-scale MBE cluster tool is shown in Fig. 1(a).[17] The system consists of a growth chamber, buffer chamber, and loading and unloading chambers. The substrate platen holds 7, six-inch diameter wafers. The platen is transferred into and out of the central distribution chamber via a manipulator arm. During a growth cycle, the platen is mounted on a substrate heater in the growth chamber facing downwards towards the Knudsen cells containing the elemental source materials. Since there are several different layers comprising the device structure, multiple effusion cells are continuously heated, with the material flux from each cell controlled by individual shutters.

Figure 1(b) shows a top schematic view of the proposed LMBE system comprising a main chamber with multiple, interconnected growth positions along a row, and loading and unloading chambers at each end. The substrate preparation and storage chambers can also be placed in-line or vertically relative to the loading and unloading chambers. The desired epitaxial structure is realized by growing layers of similar thicknesses and growth times at each position to prevent delays incurred by the entire line while a particularly thick layer is grown. For example, if the typical layer thickness required in the device is d, but the active region thickness is larger, e.g. $3d$, then each of the layers are grown at separate positions within the line, whereas the active region is grown by consecutive steps at three adjacent positions. Thus, the throughput of this example line is:

$$TP = N/(d/r + t_{tr}),\qquad\qquad(1)$$

where r is the rate of growth of a layer (in μm/h), $N = 7$ is number of wafers per platen, and t_r is the cumulative transfer time from loading, to transfer between growth sections, to unloading. Since each growth position is used to grow layers of approximately equal thickness, N wafers are produced at each the position.

Substrate platens with the same nominal size as used in a conventional MBE system are transferred in a "bucket brigade" fashion from the loading chamber, through the several growth positions, to the unloading chamber. After each layer growth, the substrates are transferred in unison from their current positions to the next position, and the growth cycle starts again. The complete multilayer structure is obtained after a platen transits the length of the system from loading to unloading. This configuration allows for increased utilization of effusion cells, and replaces multiple manipulator arms with a simple linear transfer system (see below). Each growth position consists of a substrate heater with only those effusion cells required for the growth of a

particular layer. As a consequence, the total chamber volume occupied by a growth section is smaller than that of a conventional MBE system. Therefore, supporting equipment such as pumps and electronics are shared between multiple sections.

A limitation of the LMBE architecture is that its flexibility in growing a variety of different structures is restricted, since each growth position is optimized to achieve a pre-determined layer composition within a designated device structure. Changing the number of growth positions (and hence the total number of layers) requires an extension of the main chamber. Flexibility can be improved by inserting blank effusion cells and growth sections along the system length that can be activated as needed at a low incremental expense.

Conventional MBE systems use a complex manipulator arm to transfer the substrate platen between the main growth and buffer chambers. The LMBE eliminates the need for a manipulator arm between growth sections, since platen transfer occurs via a linear movement, thereby reducing machine cost and footprint. Figure 2(a) shows a schematic of the linear transfer mechanism. A rack-and-pinion track transfers platens between growth positions distributed along the system length (the x-axis). Platen holders, or tabs, are placed in the rack at intervals equal to the distance between growth positions. Platens have protrusions, or "ears" that fit into the tabs attached to the rack. A rotating substrate heater whose axis is along the z-direction is located each growth position. A schematic of the substrate heater with sidewall openings and a substrate platen with ears is shown in Fig. 2(b).

Vertical and rotational movements of the substrate heater locks the platen into the heater by holding the platen ears in the sidewall openings (Supporting Information Video 1). Unlocking the platen from the heater entails the reverse of the locking sequence. During growth, substrate platens are held by the substrate heaters. The tabs are located at the midpoints of the growth

6

positions, as shown in Fig. 3(a). After each layer is grown, the "transfer in" step commences. The rack moves in the -x direction by half the distance between growth positions. Then the $(N+1)^{th}$ tab is aligned with N^{th} growth position (Fig. 3(b)). Substrate platen heaters move down along z-axis, leave the platen at the tabs by unlocking, and then retract. A new substrate platen is transferred from the loading chamber to the first platen holder, which is now empty. In the final step – "transfer out"— the rack moves in the +x direction by the distance between each growth position until the first platen tab is aligned with first growth position, as shown in Fig. 3(c). Once growth is complete, the platen at the end of the rack is transferred to the unloading chamber, and the rack moves in the -x direction by half the distance between growth chambers, returning to the first step of the growth cycle. A linear transfer demonstration video showing the transfer cycle for 3 adjacent growth positions is found in Supporting Information Video 2.

The number of growth positions is determined by the particular structure being grown. An example inverted GaAs single junction photovoltaic cell used for ND-ELO processing is shown in Fig. 4. The structure can be divided into three different sections: sacrificial and protection layers used to separate the epitaxy from the parent wafer, the emitter/front contact, and the base/back contact layers. The ND-ELO structure comprises a 425 nm thick sacrificial-plus-protection layer structure (blue rows). The emitter/front contact (green rows) layers are 335 nm thick, and the 2.82 μm thick base/back contact layers (yellow and orange rows) are divided into 6 identical, 470 nm thick sections to equalize the time spent growing each layer in the sequence. The growth chamber thus requires 8 growth positions starting with AlAs and InGaP sacrificial and protection layers, then the emitter layer, and 6 base layers. Figure 5 shows the LMBE chamber configuration and the 30 effusion cells required for this single junction device. The effusion cells used for each growth section are summarized in Table I.

III. Cost analysis of single junction GaAs solar cells grown by LMBE

We now estimate the system cost and ultimately the solar cell production cost for the example structure in Fig. 4. As shown in Fig. 5, the base layer growth sections require only 3 effusion cells per section, and the other sections require 5 effusion cells each. Conventional MBE growth chambers accommodate at least 10 effusion cells. The increase in chamber volume by the addition of a growth section is based on the number of effusion cells required per section. The chamber cost and required pumping capacity are assumed to be proportional to the added volume. We assume that the first and last chamber sections occupy 50% of the volume of a conventional growth chamber, with 5 effusion cells per section (see Fig. 5). Thus, the entire system volume is approximately 300% that of a conventional MBE growth chamber. Solid sources are used for all elements, and slotted stainless steel dividers are used to separate growth positions to prevent cross-contamination. For further cost reductions, the chamber walls are cooled using a closed loop polymer chiller. Previously, it has been found that there is no significant difference in the quality of GaAs grown using a chiller than a more costly liquid nitrogen-cooled chamber.[22] Maintenance and calibration costs are estimated to be twice that of a conventional MBE system, considering the increase in chamber size and number of effusion cells. Total machine costs are estimated based on conventional parts costs assuming bulk purchasing required for production equipment (see Table II).

The cost of ownership is calculated based on previous studies of large-scale, production MBE systems.[17] For conventional MBE, 0.25 unskilled and 0.09 skilled labor is required per tool.[17] For linear MBE, the same amount of skilled labor is assumed since the growth sequence can be automated. Unskilled labor is assumed to be doubled, considering the increased throughput,

maintenance and number of platens that require handling. Wages for unskilled and skilled labor of $12.05/hr and $17.56/hr with 55% benefits, and maintenance and calibration costs of $200K/year are based on a similar analysis for conventional MBE.[17] Power consumption of 135kW/h is inferred from a previous analysis.[17] This results in $75K/year by assuming an industrial electricity rate of $0.07/kWh.[23] Power supplied to chiller costs $25K/year, which compares favorably to liquid nitrogen coolant use at $60K/year.[17]

For the linear system, electricity plus chiller and maintenance costs are tripled since the number of pumps and effusion cells are increased by that amount. A total growth campaign length of 11.5 months and 11 months per year is assumed for conventional and linear MBE systems, respectively. Machine depreciation is assumed to follow a 10 year linear model. The machine cost for a conventional MBE system of $6 MM is inferred from a previous analysis.[17] A 25% discount is then applied for production-level bulk purchasing, leading to a total cost of $4.5 MM per conventional MBE tool. This was set higher than a typical bulk purchase discount of 10% to 15% for the MBE machine, since production-level MBE tools are only needed in modest numbers to satisfy the production needs of the microelectronics and communications industries. The assumptions are summarized in Table III. Additional costs incurred for taxes, insurance, wages other than manufacturing labor, etc. are not included in this analysis, and hence this should be considered to be an estimate at the low end of actual manufacturing costs.

Previous cost estimates of solar-to-electricity energy conversion using GaAs thin film photovoltaic cells grown via MOCVD[7] and D-HVPE[18] are used to estimate total cell production costs. The manufacturing process is divided into 3 principal steps. (i) Epitaxial growth, (ii) epitaxial lift-off, and (iii) device fabrication. Each consists of multiple process steps, where the cost per step is estimated from the sum of equipment, utilities, labor and materials costs. We

assume LMBE an epitaxial growth rate of 3 μm/hr, 6 min transfer time between each growth position with minimum cooling of the substrate during transfer to avoid epitaxial surface degradation, and 80% material utilization efficiency which is comparable to upside scenario for MOCVD growth.[7] Since conventional MBE requires heating effusion cells even between growths, 60% material utilization efficiency is assumed in that case.

Materials costs are calculated by multiplying the required materials cost per single platen by the number of platens produced per year. A 6 inch GaAs wafer cost with volume purchase varies from $90 - $150/wafer, depending on supplier.[7,18] For the conservative, or "base case", we assume a 1μm/hr growth rate, $150/wafer substrate cost[7], 20 X substrate reuse with $10/reuse ND-ELO processing cost, along with 70% yield and 25% power conversion efficiency. The more aggressive upside case assumes a 3 μm/hr growth rate, $90/wafer substrate cost[18], an upper realistic limit of 50 X substrate reuse, with $1/reuse ND-ELO processing cost along with 95% yield and 29% power conversion efficiency. Cost estimations for cell fabrication following epitaxial growth are obtained from Woodhouse, et al.[7], since the fabrication process is unaffected by the particular growth technology employed. Cost estimates for module production based on conventional and linear MBE systems are summarized in Table IV. Epitaxial growth costs are calculated based on the tool capital expense, material utilization factor and the cost of each layer in the structure[7]. Equipment cost is the sum of machine depreciation and maintenance cost. The cost contribution for each part of the process is converted from $/MBE/year to $/Wp by dividing the cost of ownership by the total solar cell power produced per tool per year. The total estimated cost including substrate cost for conventional MBE with base case assumptions, and for LMBE with both base and upside case assumptions are given in Fig. 6. The base case costs are reduced from

$24.82 to $13.63 by switching from MBE to LMBE. Upside case assumptions with optimized processes, improved cell efficiency, and lower substrate cost results in a cost of $3.67/Wp.

IV. Discussion

The foregoing discussion principally focuses on scaling conventional MBE into a continuous growth platform, allowing us to avoid uncertainties related to proposing an entirely new growth concept. Indeed, the only new (and as yet untested) component is the linear transfer mechanism in the main chamber. Given an acceptable level of market pull, we expect relatively quick development of the proposed concept after calculating the optimum distance between growth sections that can prevent cross-contamination of the epitaxial layers.

Our analysis shows that the solar-to-electricity conversion cost of GaAs PV cells can be cut by nearly 50% when a conventional MBE system is replaced with the proposed LMBE system. This primarily results from the substantial savings in capital expense and increased throughput. Labor cost in $/Wp is also reduced for LMBE due to its higher throughput. For conventional MBE with base case assumptions, most of the cell cost is determined by substrate and equipment costs. With LMBE, the equipment cost is reduced from $13.34/Wp to $4.17/Wp. Expanding the growth chamber into multiple sections reduces the components count compared to conventional MBE systems. Thus, the equipment cost and depreciation scales more slowly compared to simply multiplying the number of MBE cluster tools. Yet the substrate cost of $7.52/Wp remains unchanged regardless of growth technology employed. With upside case assumptions, the cell cost is further reduced to $3.67/Wp, which is a nearly 85% reduction compared to the estimated cost based on conventional MBE systems.

A comparison between cell costs achieved using linear MBE, MOCVD[7] or D-HVPE[18], is provided in Table V. To make this comparison, we have relied on and modified previous estimates that are not always directly comparable, and that often made unsupported assumptions. Where possible, we have attempted to make these previous estimates consistent with our current analysis, especially for substrate costs that depend on the number of reuses via ND-ELO or CMP. Our analysis assumes 50 X reuse with a cost of $1/reuse and a 29% cell efficiency, which results in $0.76/Wp substrate cost. Woodhouse, et al[7] predicts $4.6/Wp upside case cell cost grown via MOCVD, with 500 X substrate reuse and 20 μm/hr growth rate. Since current status of MOCVD can achieve a GaAs growth rate of 60 μm/hr[24], we estimate a $3.5 − 4.5/Wp considering cost reductions via this faster growth and an adjusted more realistic substrate reuse of 50X.

Analyses based on D-HVPE[18] assumed the growth of a dual junction GaInP/GaAs photovoltaic cell, making a direct comparison with the current work problematic. Furthermore, steps used that lead to bottom line estimates for D-HVPE were not provided. Nevertheless, we can draw some conclusions from those earlier estimates. Horowitz, et al. [18] estimate a $2.0/Wp cell cost of 30% efficiency, low cost Ni/Ag contacts, $90/substrate with 25 reuses and $10/CMP after every 5 reuses. However, this underestimates substrate cost, which is a major determinant of the cell cost. Including more realistic estimates, we find an upside cost of $2.50 - 3.00/Wp.

Indeed, for all the cases, the two major contributions to the cost are substrate cost and growth tool depreciation (see Table V). Cost reductions in machine depreciation are achieved by improved material utilization efficiency, faster growth rates, and optimized photovoltaic cell structure. However, by employing LMBE, the cost of epitaxial growth by all technologies are, to within the unavoidable uncertainties inherent in such analyses, equal and is no longer the primary factor governing the cost of GaAs cell manufacture.

V. Conclusion

In summary, we propose a linear MBE system configuration that has the potential to increase the wafer throughput compared to conventional MBE. This approach potentially increases the material utilization efficiency, requires fewer components compared to a conventional MBE system, while significantly increasing throughput. We estimate a nearly 55% cost reduction in the production of GaAs thin-film photovoltaic cells using LMBE compared to conventional MBE, and further reduction to 85% for optimized processes. With high volume manufacturing reaching to hundreds of MW to GW production demands, substrate and equipment costs can be further reduced compared to the estimates provided here.

Even with these optimistic assumptions, cost of materials, utilities and maintenance still remain above $3.00/Wp, regardless of the growth technology employed. Major cost impacts arise from high substrate cost that can only be reduced by improved substrate recycling techniques, rather than by increased growth rate or optimized processing. Thus, it is unlikely that MW to GW scale production demands will emerge for GaAs photovoltaics. Moreover, considering that the analyses presented here do not include taxes, insurance, labor beyond manufacturing, marketing, rent, etc., we can expect the final cost will be higher than this estimation. This makes the high demand on GaAs solar energy conversion even more difficult to compete with other incumbent technologies such as Si. Nevertheless, for applications where light weight, very high efficiency, or cell flexibility are essential (e.g. for area-constrained or aerospace applications), GaAs photovoltaics will continue to fill a niche that is inaccessible to low cost, commodity Si solar cells. In that case, LMBE provides an opportunity for cost reductions that have not been possible using conventional growth technologies.

14

References

1   NREL, Best research-cell efficiency chart, https://www.nrel.gov/pv/assets/pdfs/best-research-cell-efficiencies.20190802.pdf, (accessed 2 August 2019).

2   G. J. Bauhuis, P. Mulder, E. J. Haverkamp, J. J. Schermer, E. Bongers, G. Oomen, W. Köstler and G. Strobl, *Prog. Photovoltaics Res. Appl.*, 2010, **18**, 155–159.

3   K. Lee, J. D. Zimmerman, T. W. Hughes and S. R. Forrest, *Adv. Funct. Mater.*, 2014, **24**, 4284–4291.

4   K. Lee, J. Lee, B. A. Mazor and S. R. Forrest, *Light Sci. Appl.*, 2015, **4**, e288.

5   R. Tatavarti, G. Hillier, A. Dzankovic, G. Martin, F. Tuminello, R. Navaratnarajah, G. Du, D. P. Vu and N. Pan, in *2008 33rd IEEE Photovolatic Specialists Conference*, IEEE, 2008, pp. 1–4.

6   K. A. Horowitz, T. W. Remo, B. Smith and A. J. Ptak, A Techno-Economic Analysis and Cost Reduction Roadmap for III-V Solar Cells, http://www.osti.gov/servlets/purl/1484349/, (accessed 3 September 2019).

7   M. Woodhouse and A. Goodrich, A Manufacturing Cost Analysis Relevant to Single- and Dual-Junction Photovoltaic Cells Fabricated with III-Vs and III-Vs Grown on Czochralski Silicon, https://www.nrel.gov/docs/fy14osti/60126.pdf, (accessed 3 September 2019).

8   J. S. Ward, T. Remo, K. Horowitz, M. Woodhouse, B. Sopori, K. VanSant and P. Basore, *Prog. Photovoltaics Res. Appl.*, 2016, **24**, 1284–1292.

9   S. W. Bedell, D. Shahrjerdi, B. Hekmatshoar, K. Fogel, P. A. Lauro, J. A. Ott, N. Sosa and D. Sadana, *IEEE J. Photovoltaics*, 2012, **2**, 141–147.

10   C. A. Sweet, K. L. Schulte, J. D. Simon, M. A. Steiner, N. Jain, D. L. Young, A. J. Ptak and C. E. Packard, *Appl. Phys. Lett.*, 2016, **108**, 011906.

11   N. Jain, D. Crouse, J. Simon, S. Johnston, S. Siol, K. L. Schulte, C. E. Packard, D. L. Young and A. J. Ptak, *IEEE J. Photovoltaics*, 2018, **8**, 1384–1389.

12   S. A. Hadi, E. A. Fitzgerald, S. Griffiths and A. Nayfeh, *J. Renew. Sustain. Energy*, 2018,

10, 015905.

13   M. Yamaguchi, A. Yamamoto and Y. Itoh, *J. Appl. Phys.*, 1986, **59**, 1751–1753.

14   C. L. Andre, J. J. Boeckl, D. M. Wilt, A. J. Pitera, M. L. Lee, E. A. Fitzgerald, B. M. Keyes and S. A. Ringel, *Appl. Phys. Lett.*, 2004, **84**, 3447–3449.

15   K. Lee, C.-W. Chien, B. Lee, A. Lamoureux, M. Shlian, M. Shtein, P. C. Ku and S. Forrest, *ACS Photonics*, 2016, **3**, 2134–2140.

16   S. P. Philipps, A. W. Bett, F. Institute for Solar Energy Systems ISE, K. Horowitz, S. Kurtz and N. Renewable Energy Laboratory NREL, .

17   M. O'Steen, E. Readinger, M. Doran and D. Hanser, *Systems and technology for production-scale molecular beam epitaxy*, Elsevier, 2013.

18   K. A. Horowitz, T. W. Remo, B. Smith and A. J. Ptak, A Techno-Economic Analysis and Cost Reduction Roadmap for III-V Solar Cells.

19   W. Metaferia, K. L. Schulte, J. Simon, S. Johnston and A. J. Ptak, *Nat. Commun.*, , DOI:10.1038/s41467-019-11341-3.

20   K. L. Schulte, J. Simon and A. J. Ptak, *Prog. Photovoltaics Res. Appl.*, , DOI:10.1002/pip.3027.

21   D. Feldman, N. Anna Ebers and D. Robert Margolis, Q3/Q4 2018 Solar Industry Update, https://www.nrel.gov/docs/fy19osti/73234.pdf, (accessed 28 May 2019).

22   R. B. Lewis, J. A. Mackenzie, T. Tiedje, D. A. Beaton, M. Masnadi-Shirazi, V. Bahrami-Yekta, K. P. Watkins and P. M. Mooney, *J. Vac. Sci. Technol. B, Nanotechnol. Microelectron. Mater. Process. Meas. Phenom.*, 2013, **31**, 03C116.

23   U.S. Energy Information Administration, Average price of electricity to ultimate customers by end-use sector, https://www.eia.gov/electricity/monthly/epm_table_grapher.php?t=epmt_5_6_a, (accessed 12 September 2019).

24   H. Sodabanlu, A. Ubukata, K. Watanabe, T. Sugaya, Y. Nakano and M. Sugiyama, *IEEE J. Photovoltaics*, 2018, **8**, 887–894.

Table I. Effusion cells required for different layers.

Layer	Material	K-cell sources	Number of layers	Number of K-cell sources
ELO structure	GaAs, GaInP, AlAs	In, Ga, Al, As, P	1	5
Emitter, Top contact	GaAs(n), GaInP(n)	In, Ga, As, P, Si	1	5
Base	GaAs(p)	Ga, As, Zn	5	3
Base, Bottom contact	GaAs(p), AlGaAs(p)	Ga, Al, As, Zn, C	1	5

Table II. Cost estimation based on machine parts.

Part	Unit cost	# of units	Total cost
End chambers	$200K	2	$400K
Chamber sections-emitter	$200K	1	$200K
Chamber sections-base	$120K	5	$600K
Linear transfer system	$50K	1	$50K
Transfer arm for loading / unloading	$50K	2	$100K
Loading / buffer chamber	$100K	2	$200K
Main chamber pump	$30K	3	$90K
Buffer chamber pump	$15K	2	$60K
K-cell with controller, power supply	$100K	30	$3.0M
Electronics, measurement tools	$200K	-	$200K
Cost	-	-	$4.9 MM
Price (Total + 40% margin)	-	-	$6.9 MM

Table III. Assumptions for MBE cost of ownership estimation

MBE Cost	Unit	Conventional MBE	Linear MBE
Thickest section thickness	μm	3.574	0.47
Substrates / platen	/MBE	7	
Unskilled labor	/MBE	0.25	0.5
Skilled labor	/MBE	0.09	0.09
Unskilled wage	$/MBE/year	39200	75100
Skilled wage	$/MBE/year	20600	19700
Cycled chiller + Electricity	$/MBE/year	100000	300000
Materials utilization		60%	80%
Maintenance + Calibration	$/MBE/year	200000	600000
Depreciation	$/MBE/year	450000	690000
Campaign Length	Month	11.5	11
Maintenance Time	Month	0.5	1

Table IV. Cost estimation based on conventional and linear MBE.

Step	Equipment ($/Wp)	Utilities ($/Wp)	Labor ($/Wp)	Materials ($/Wp)	Substrate ($/Wp)
Epitaxial growth (Conventional MBE)	13.17	1.01	1.21	0.06	7.52
Epitaxial growth (Linear MBE)	3.99	0.46	0.29	0.06	7.52
Epitaxial growth (Linear MBE, upside)	1.55	0.18	0.11	0.04	0.76
Anode metallization + Bond to flexible substrate	0.02	0.005	0.01	0.225	
Dissolve sacrificial layer + lift-off cell	0.018	0.001	0.008	0.02	
Prep substrate (plasma clean)	0.015	0.0005	0.0005	0.006	
Prep substrate (etch protection layer)	0.018	0.001	0.008	0.02	
Etch front side	0.018	0.001	0.008	0.02	
Cathode metallization	0.024	0.001	0.006	0.046	
VTE ARC	0.015	0.0005	0.0005	0.006	
Test + sort	0	0	0.05	0	
Build module	0.05	0.06	0.06	0.1	
Total (Conventional MBE)	13.34	1.08	1.36	0.5	7.52
Total (Linear MBE, base case)	4.17	0.53	0.44	0.5	7.52
Total (Linear MBE, upside case)	1.73	0.25	0.26	0.48	0.76

Table V. Comparison between MBE, LMBE, MOCVD and D-HVPE

	Maximum growth rate (μm/hr)	No. wafers / hr	Material utilization efficiency	Technology status	Precursor required	Solar cell cost (upside case)	Reference
MBE	3	7	60 - 80%	used in industry	elemental	$8.8/Wp	13
LMBE	3	27	60 - 80%	proposed	elemental	$3.67/Wp	This work
MOCVD	50-60	100 - 120	30 - 50%	used in industry	metalorganic	$3.50 - 4.50/Wp	9
D-HVPE	200	200 - 300	60 - 80%	lab scale demo.	elemental	$2.50 - 3.00/Wp	8

Figure captions

Figure 1: (a) Schematic illustration of a top view of a conventional production scale MBE machine comprising a distribution chamber, growth chamber and small peripheral chambers. (b) Proposed linear MBE machine with expanded growth chamber.

Figure 2: (a) Schematic illustration of a rack and pinion linear transfer system with tabs attached to the rack and substrate heaters at growth positions. (b) Substrate heater and platen, showing the range of motion of the heater for picking up and laying down of platen.
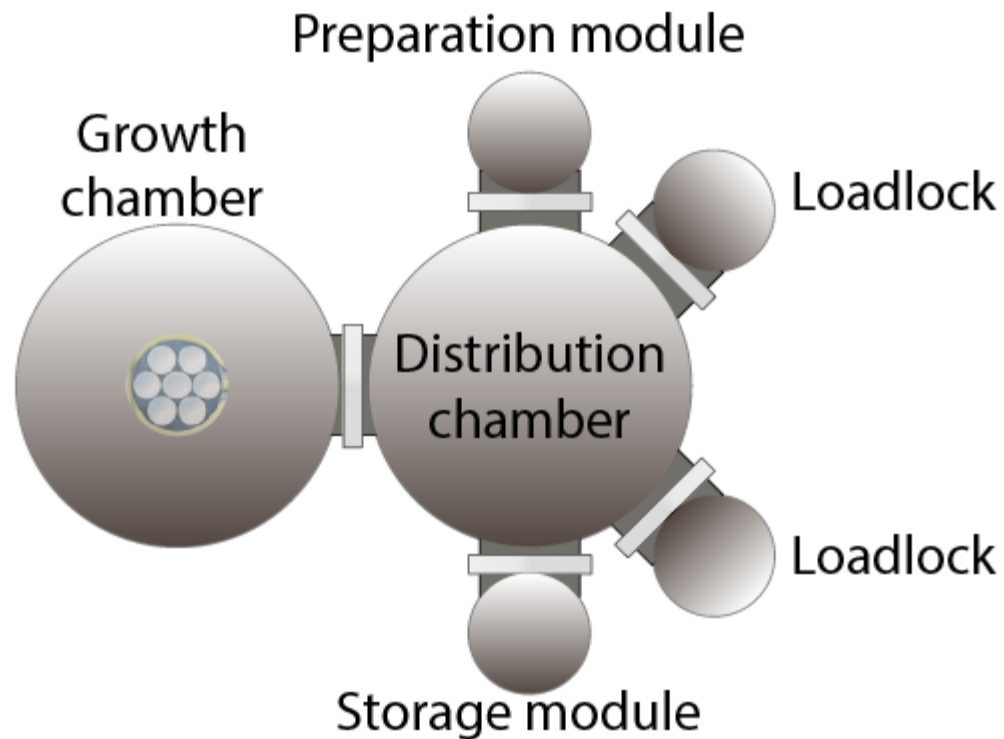
Figure 3: Schematic illustration of a linear transfer system, with rack at (a) the growth position, (b) the transfer into the growth position, shifted by half the distance between growth positions in the backwards direction, and (c) the transfer-out position, shifted by the distance between growth positions in the forward direction.

Figure 4: An inverted single junction GaAs photovoltaic cell structure used for analysis. The sacrificial layer used in epitaxial lift off with protection layers (blue), emitter and front contact layers (green), base layers (yellow) and back contact layers (orange) are indicated.
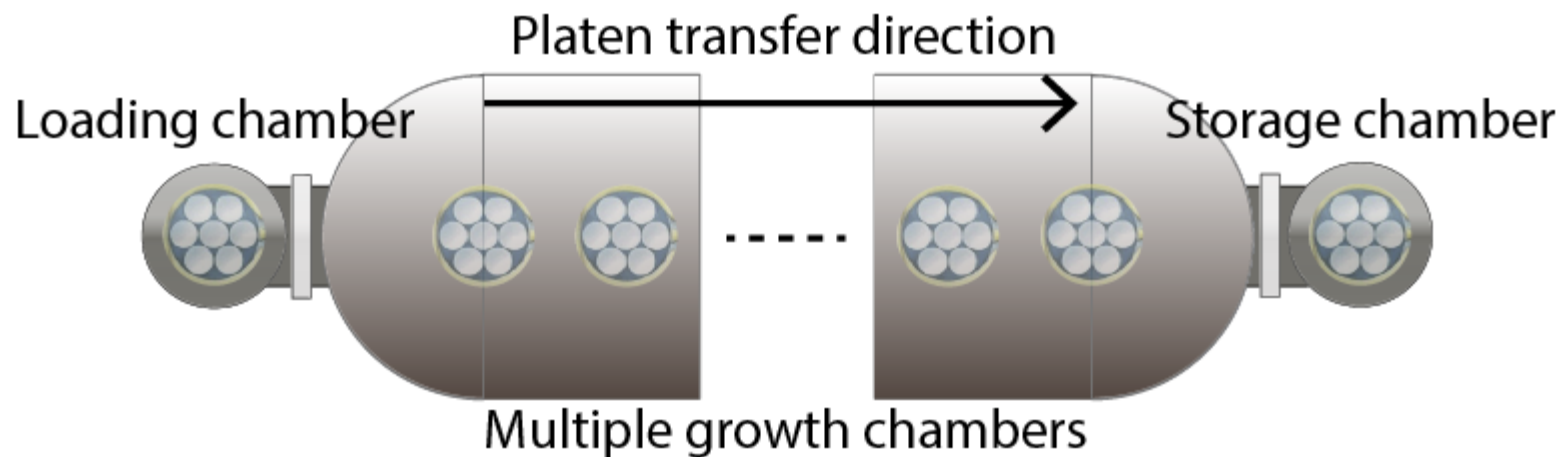
Figure 5: Schematic illustration of linear MBE system chamber configuration designed for growth of inverted single junction GaAs photovoltaic cells with the number of required effusion cells at each growth position.

23

Figure 6: GaAs photovoltaic cell cost estimation for three cases: growth via conventional MBE, linear MBE with base case assumptions, and linear MBE with upside case assumptions.
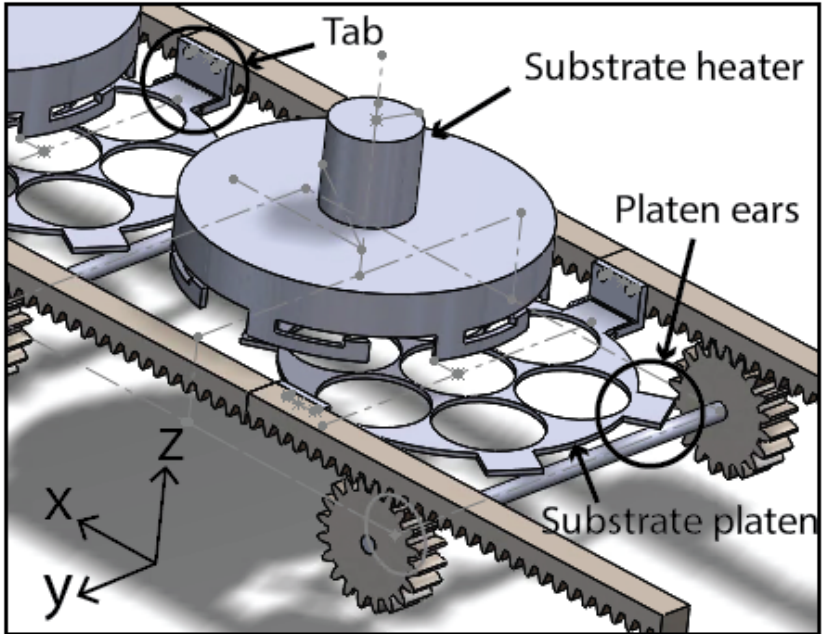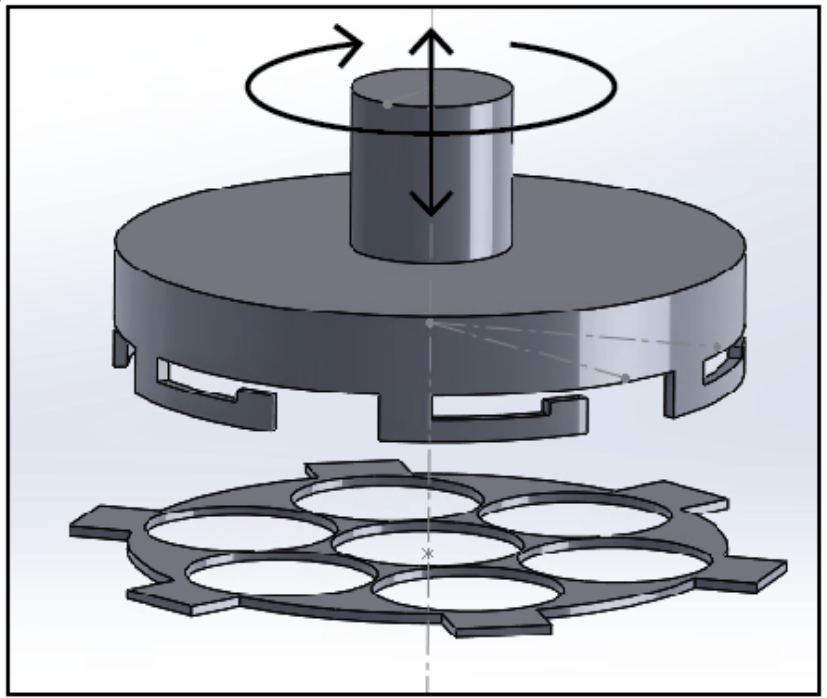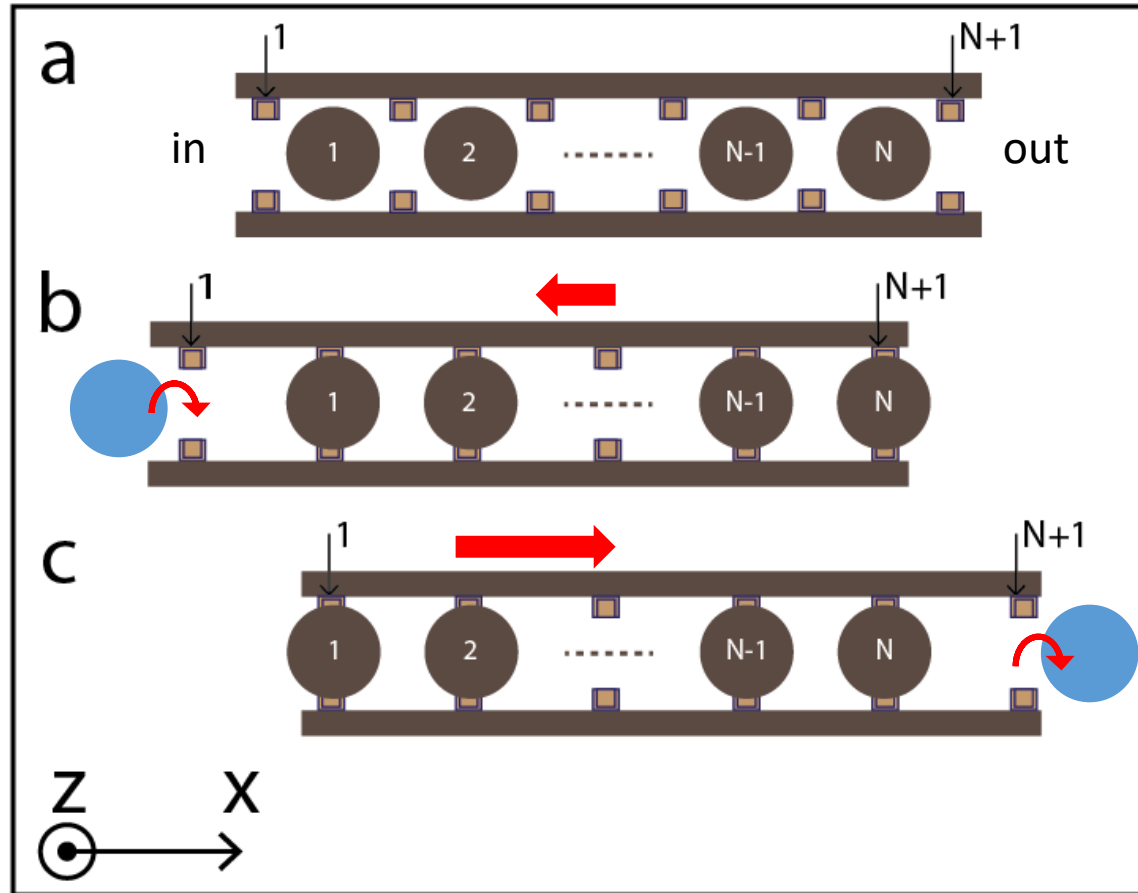
a

Growth
chamber

Preparation module

Loadlock

Distribution
chamber

Loadlock

Storage module

b

Platen transfer direction

Loading chamber

Storage chamber

Multiple growth chambers

Thickness (nm)	Material	Description	Dopant	Layer type	Growth position
15	GaAs	Contact (p++)	C	Back contact	8
20	GaAs	Contact (p+)	Zn		
100	Al(0.26)GaAs	BSF (p+)	C		
2500	GaAs	Base (p+)	Zn	Base	3~7
34	GaAs	NID	-	Emitter / Top contact	2
150	GaAs	Emitter (n+)	Si		
25	Ga(0.49)InP	Window (n+)	Si		
100	GaAs	Setback (n+)	Si		
25	GaAs	Contact (n++)	Si		
50	Ga(0.49)InP	Etch Stop	-	Epitaxial lift-off structure	1
100	GaAs	Protection	-		
25	AlAs	Release Layer	-		
100	GaAs	Protection	-		
50	Ga(0.49)InP	Etch Stop	-		
100	GaAs	Buffer	-		